MATERIALS CHEMISTRY
FRONTIERS

RESEARCH ARTICLE

View Article Online
View Journal | View Issue

Cite this: *Mater. Chem. Front.*, 2019, **3**, 2738

Supramolecular polymerization and cyclization of dioxynaphthalene motif bridged bifunctional UPys: minor variations in the molecular skeleton and drastic differences in self-assembly†

Tangxin Xiao, *[a] Lixiang Xu,[a] Julian Götz,[b] Ming Cheng,[c] Frank Würthner, *[b] Jiande Gu,[a] Xuejun Feng,*[a] Zheng-Yi Li,[a] Xiao-Qiang Sun[a] and Leyong Wang *[ac]

Received 24th September 2019,
Accepted 9th October 2019

DOI: 10.1039/c9qm00595a

rsc.li/frontiers-materials

The relationship between molecular structure and macroscopic characteristics is a fundamental issue for materials design. Some minor changes in molecular structure may have a great impact on the molecular self-assembly process. Therefore, it is of interest to design new isomeric building blocks for supramolecular self-assembly, offering inspiration for the development of smart materials by supramolecular engineering. In this study, two dioxynaphthalene (DNP) group bridged bifunctional ureidopyrimidinone (UPy) monomers (**DNP1** and **DNP2**) were synthesized. The chemical structures of the two isomers are very similar and the only difference is that **DNP1** is 2,6-substituted and **DNP2** is 1,5-substituted on the DNP motif. Interestingly, these two isomers exhibit completely different supramolecular self-assembly behaviors. Highly viscous supramolecular polymers were obtained in a concentrated solution of **DNP1**, while crystals based on highly stable cyclic monomers were precipitated from a concentrated solution of **DNP2**. Since DNP is an electron rich group, the host–guest behaviors of **DNP1** and **DNP2** with a blue-box were further studied, which also showed different ring-threading capabilities.

Introduction

Scientists have long endeavored to comprehend the interplay between non-covalent and covalent bond formation, in order to study and understand how function is related to self-assembly.[1–4] Moreover, minor changes in molecular structure may impact the inherent molecular properties and further transfer this difference to the final assemblies.[5] Therefore, controlling the linking sequence of groups in one molecule is a potential alternative method to adjust the function of its corresponding supramolecular materials. Supramolecular polymers, in which low molecular weight monomers are assembled into polymeric structures by non-covalent interactions, attract much interest due to their highly tunable functional groups and dynamic nature.[6–9] So far, supramolecular polymerization controlled by different means have been established, such as pathway control,[10,11] orthogonal self-assembly,[12–14] living supramolecular polymerization,[15,16] *etc.* Meanwhile, a large number of advanced supramolecular polymers with excellent properties have been developed by using various non-covalent interactions as a driving force, including macrocycle-based host–guest interactions,[17,18] multiple hydrogen bonding,[19,20] metal–ligand coordination,[21,22] or integration of these forces.[23–25] On the one hand, obtaining a supramolecular polymer with a high degree of polymerization is one of the goals of developing practical supramolecular materials. On the other hand, optimization of discrete aggregates with well-defined architectures in self-assembled systems is also one of the targets of supramolecular chemists.[26,27] Therefore, it would be interesting for the final assemblies to shift between highly viscous supramolecular polymers and well-defined discrete cyclic oligomers *via* minor structural adjustments in the molecule.

The ureidopyrimidinone (UPy) unit which can undergo quadruple hydrogen bonding is a promising supramolecular building block owing to its high dimerization constant ($K_{dim} > 10^7$ M^{-1} in chloroform), self-complementary nature, and ease of synthesis.[28,29] In recent years, a large amount of supramolecular polymers[30–35] and well-defined supramolecular assemblies based on UPy have been constructed.[36,37]

[a] *Jiangsu Key Laboratory of Advanced Catalytic Materials and Technology, School of Petrochemical Engineering, Changzhou University, Changzhou, 213164, China. E-mail: xiaotangxin@cczu.edu.cn, xuejun-f@163.com*
[b] *Universität Würzburg, Institut für Organische Chemie & Center for Nanosystems Chemistry, Am Hubland, 97074 Würzburg, Germany. E-mail: wuerthner@uni-wuerzburg.de*
[c] *School of Chemistry and Chemical Engineering, Nanjing University, Nanjing, 210023, China*

† Electronic supplementary information (ESI) available: Experimental details, additional NMR spectra, and HR-ESI-MS spectra of individual compounds. See DOI: 10.1039/c9qm00595a

By connecting two UPy units to tetraphenylethene motif, Tang and co-workers found that the supramolecular polymerizabilities and fluorescence properties of the stereoisomers depend strongly on the configuration of the molecules.[38] Additionally, the π–π stacking interaction also plays a key role in supramolecular self-assembly.[39,40] It is noteworthy that the UPy motif can not only dimerize through quadruple hydrogen bonding but also exhibit π–π stacking capability with aromatic groups.[41,42]

Previously, Zhang and co-workers synthesized 1,5-substituted and 2,6-substituted dioxynaphthalene (DNP)-based amphiphiles, both of which could complex with electron-deficient naphthalene diimide group-based amphiphiles through charge-transfer interactions to form supra-amphiphiles, leading to the further formation of rod-like and sheet-shape nanostructures, respectively.[43] Based on the above mentioned appealing examples and encouraged by our experiences on various non-covalent interactions,[44–46] we attempted to combine UPy and DNP groups to fabricate supramolecular assemblies with various topological architectures, so as to deepen the understanding of the relationship between molecular structures and supramolecular self-assembly. As shown in Fig. 1, two kinds of DNP-bridged bifunctional UPy monomers (**DNP1** and **DNP2**) were designed and synthesized. The chemical structures of the two monomers are similar and the only difference is that **DNP1** is substituted in the 2,6-position, while **DNP2** is substituted in the 1,5-position on the DNP moiety. According to the ring-chain equilibrium mechanism, there is a critical polymerization concentration (CPC) upon concentration increase in the ring-opening polymerization process of bifunctional UPys,

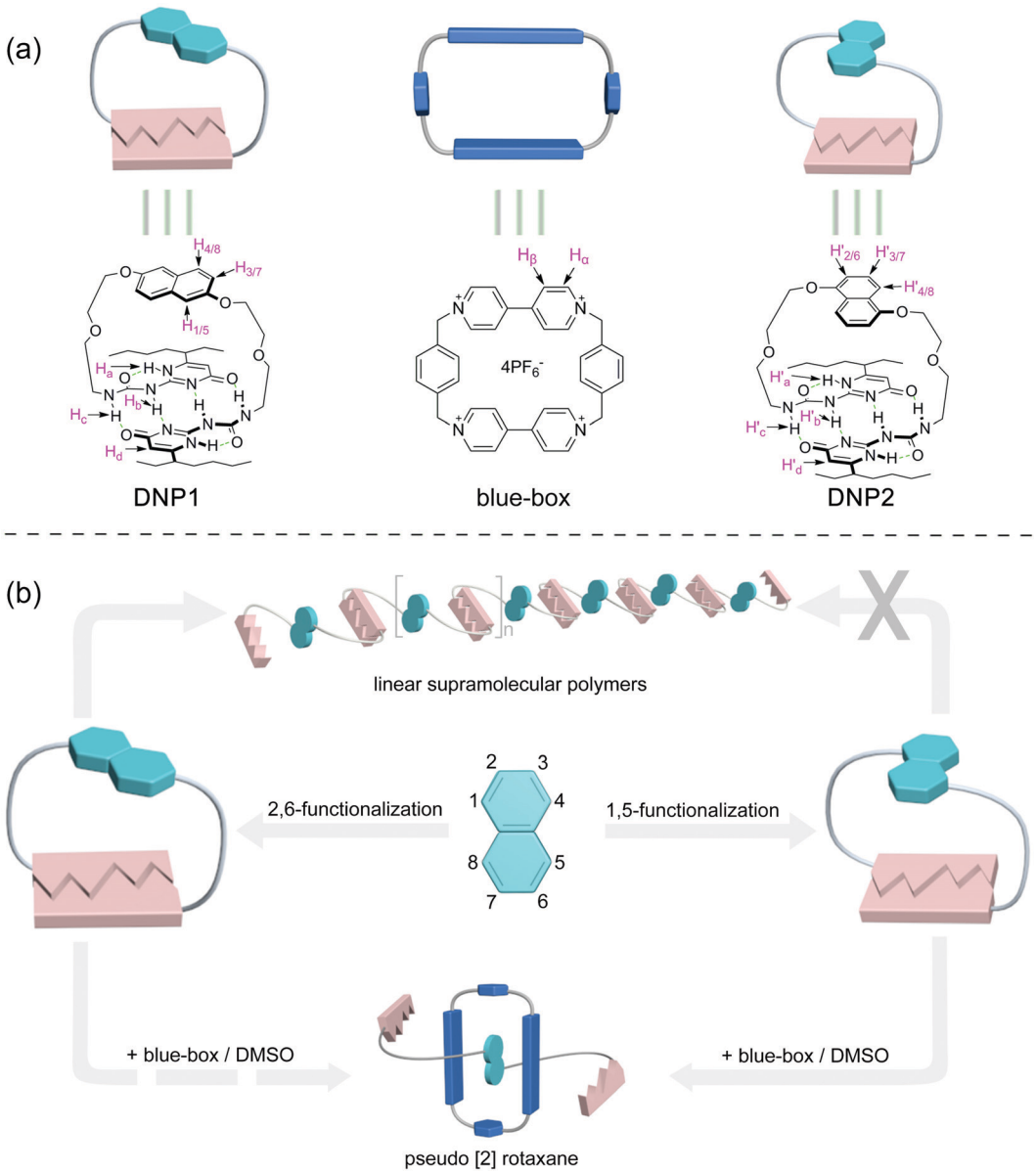

Fig. 1 (a) Chemical structures and cartoon representations of **DNP1**, **DNP2**, and the blue-box, and (b) schematic illustration of the supramolecular polymerizability of **DNP1** and **DNP2**, and their potential host–guest behaviors with the blue-box.

suggesting that the cyclic monomer is predominantly below the CPC and linear polymers are the main species above the CPC in solution.[47] This study shows that the self-assembly behaviors of **DNP1** and **DNP2** are totally different although they have similar molecular structure. Monomer **DNP1** exhibited typical ring-opening supramolecular polymerization behavior and a highly viscous supramolecular polymer was obtained. In stark contrast, **DNP2** could not open its ring and maintained an extremely stable cyclic monomer structure throughout the concentration range (0–650 mM), resulting in precipitation of crystals from its concentrated solution. Herein, the ring tension and the π–π interaction in their cyclic monomer play important roles in the self-assembly process. Moreover, mechanically interlocked molecules have drawn much interest in recent years.[48–50] Since the DNP group is electron rich, the different self-assembly behaviors of **DNP1** and **DNP2** with electron-deficient cyclobis(paraquat-*p*-phenylene)cyclophane (the so-called "blue-box") have also been explored.

Results and discussion

The DNP bridged bifunctional UPy compounds **DNP1** and **DNP2** have been designed (Fig. 1). The synthesis of these UPys is straightforward (see the ESI,† Scheme S3). The starting materials are 1,5-naphthalenediol and 2,6-naphthalenediol, respectively. After a few steps of simple reaction, two DNP group bridged ditopic terminal amine compounds were obtained. Connecting the amine compounds with 1,1′-carbonyldiimidazole activated pyrimidinone (UPy precursor) afforded **DNP1** and **DNP2**. All the compounds were thoroughly characterized by NMR and mass spectrometry.

The supramolecular polymerizability of **DNP1** and **DNP2** was first studied by ^{1}H NMR upon varied monomer concentrations. The chemical shifts of the N–*H* proton signal in the two monomers are shifted significantly downfield (9.5–13.5 ppm) in $CHCl_3$, indicating the formation of quadruple hydrogen bonding. As shown from the ^{1}H NMR spectra of **DNP1** (Fig. 2a), only one set of peaks (marked by red dots) indicates the presence of the cyclic monomer below 350 mM. However, a new set of peaks representing the cyclic dimer appeared upon increasing the concentration (marked by blue squares, see Fig. 6 for further discussion). As the concentration continues to increase, another new set of peaks (marked by green triangles) representing the linear supramolecular polymers occurred. During this process (Fig. 2a, 350–650 mM), the intensity of the polymer peaks increased and their shape became broad gradually. These phenomena suggest that **DNP1** follows a typical ring-chain equilibrium supramolecular polymerization mechanism. Subsequently, a CPC value of 347 mM for **DNP1** was calculated based on H_b by plotting the cyclic species concentration *versus* the total monomer concentration (see the ESI,† Fig. S3). Compared with other bifunctional UPys, the CPC of **DNP1** is relatively high. This might be due to the π–π stacking interaction between dimerized UPy and DNP groups, which can stabilize the structure of the cyclic monomer and inhibit the ring-opening to some extent.[13] It is

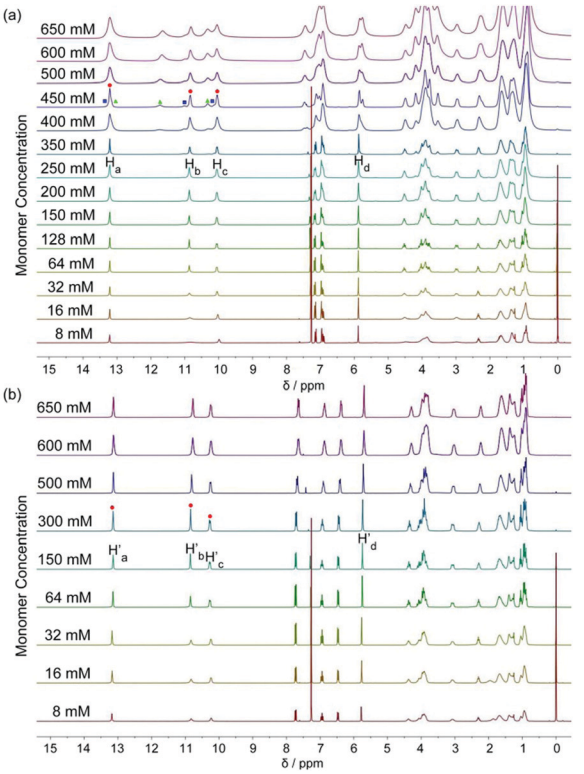

Fig. 2 ^{1}H NMR spectra (300 MHz, $CDCl_3$, 298 K) of (a) **DNP1** and (b) **DNP2** at different monomer concentrations. The red dots indicate cyclic monomers and the blue squares stand for cyclic dimers and the green triangles represent polymeric assemblies.

worth noting that H_b and H_c, both of which are involved in quadruple hydrogen bonding, showed obvious downfield shifts (from 10.82 to 11.00 to 11.70 ppm for H_b, from 10.03 to 10.13 to 10.32 ppm for H_c) upon ring-opening polymerization, indicating the stepwise loss of shielding effect between the dimerized UPy motif and DNP moiety. The peaks of H_a and H_d shifted a little upfield during polymerization, indicating that H_a and H_d were located at the peripheral domain of the DNP group, which is consistent with the structure model of the cyclic monomer.

In contrast to **DNP1**, **DNP2** exhibited a completely different self-assembly behavior. As shown in Fig. 2b, only one set of peaks appeared during the whole concentration range (8–650 mM) and no new peaks occurred even in the highest measurable concentration (650 mM). Higher concentration solutions are not suitable for NMR due to the limited solubility of the compound. Notably, the peaks were still sharp even at 650 mM, indicating that no polymeric species were generated. These phenomena suggested that **DNP2** existed in the form of a very stable cyclic monomer in solution and no CPC was found, which showed a dramatic difference with **DNP1**. **DNP2** did not show ring-opening supramolecular polymerization behavior mainly due to the stronger π–π interaction between the DNP moiety and the dimerized UPy motif, which greatly enhanced the stability of the monomeric structure.[13] Compared to **DNP2**, the ring-strain of 2,6-substituted **DNP1** is much larger than the one of **DNP2**, which favors the ring-opening of **DNP1**. It can be understood as

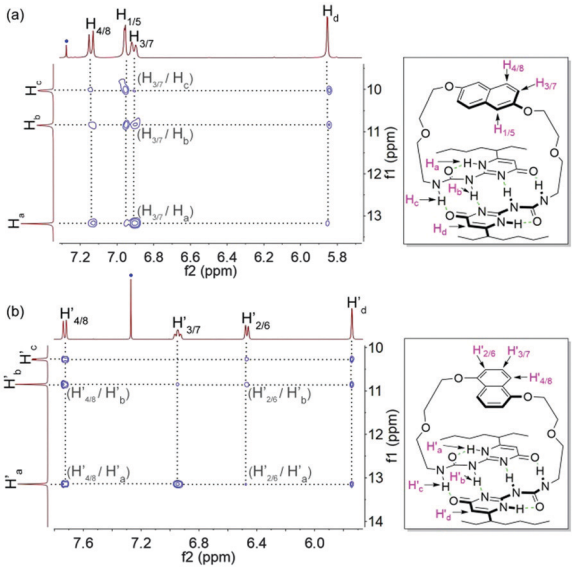

Fig. 3 Partial NOESY (400 MHz, $CDCl_3$, 298 K) of (a) **DNP1** (64 mM) and (b) **DNP2** (64 mM). The blue dots indicate solvent peaks.

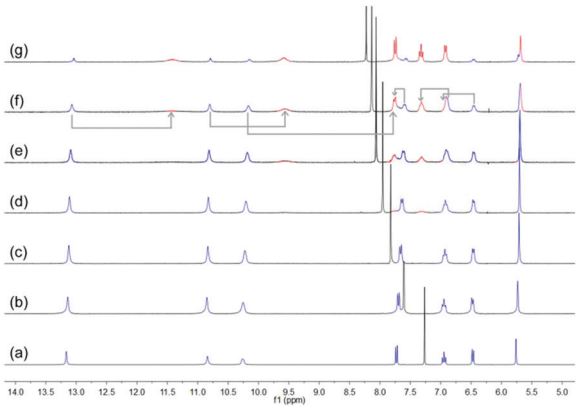

Fig. 4 Partial ^{1}H NMR spectra (300 MHz) of **DNP2** (16 mM) in mixed $CDCl_3$/DMSO-d_6 solvents. From bottom to top: χ_{DMSO} = (a) 0, (b) 0.17, (c) 0.29, (d) 0.38, (e) 0.47, (f) 0.58 and (g) 0.71. Blue peaks stand for cyclic monomers and red peaks originate from open monomers.

follows: (1) the positions of the building blocks DNP and UPy of the two monomers in space are fixed, (2) the diethylene glycol linkers play the role of a ''rope'' to bundle the DNP and UPy building blocks together, (3) the length of the ''rope'' is the same, but **DNP1** is 2,6-substituted and causes the tension of the rope to increase.

The monomeric form of **DNP1** and **DNP2** was further evidenced by NOESY NMR. A solution of **DNP1** in $CDCl_3$ at 64 mM, which is far from its CPC, was employed for measurement. As expected, strong NOE signals occurred between DNP protons ($H_{1/5}$, $H_{3/7}$, and $H_{4/8}$) and UPy N–*H* protons (H_a, H_b, and H_c) (Fig. 3a). Additionally, obvious correlations were also observed between the protons from the 1-ethylpentyl group of the UPy and DNP protons ($H_{1/5}$, $H_{3/7}$, and $H_{4/8}$) (see the ESI,† Fig. S1). All these correlations indicate that **DNP1** indeed prevails as a cyclic monomer architecture through intramolecular quadruple hydrogen bonding of UPy at the current concentration (64 mM). The NOESY of **DNP2** exhibited similar results, which also proved that **DNP2** exists in its cyclic monomer form. Obvious NOE correlations were observed between DNP protons ($H'_{2/6}$, $H'_{3/7}$, and $H'_{4/8}$) and UPy N–*H* protons (H'_a, H'_b, and H'_c) (Fig. 3b) as well as protons from the 1-ethylpentyl chain (see the ESI,† Fig. S2).

The self-assembly behaviors of **DNP1** and **DNP2** were further tested by temperature-dependent ^{1}H NMR. The concentration of **DNP1** was set at 350 mM, which was close to its CPC value. As shown in Fig. S4 (see the ESI†), the peaks belonging to the polymer species are gradually increased and become broad as the temperature increases from 298 K to 333 K, indicating that the cyclic monomer of **DNP1** is not stable enough and would undergo ring-opening supramolecular polymerization as the temperature increases. Under the same conditions, **DNP2** exhibited totally different behavior. It can be seen from Fig. S5 (see ESI†) that as the temperature increases from 298 K to 333 K, no new peaks appear and the original peaks remain sharp, showing that the cyclic monomer of **DNP2** is very stable even at high temperature. These observations again confirmed the drastic differences between **DNP1** and **DNP2** in their self-assembly processes.

Subsequently, the stability of **DNP1** and **DNP2** in their cyclic monomer form was studied in $CDCl_3$ with the addition of DMSO-d_6 which is a strong hydrogen bond breaking solvent. As χ_{DMSO} (percentage of volume) increased to above 0.38, a new set of small peaks representing the open form of **DNP2** appeared (Fig. 4). Compared with other UPys that usually start to dissociate at $\chi_{DMSO} < 0.1$,[51] the cyclic form of **DNP2** is much more stable. The simultaneous presence of two sets of peaks indicates that the equilibrium between open form and closed form of monomeric **DNP2** is in a slow exchange regime on the time scale of NMR. As the amount of DMSO continued to increase, the proportion of open monomers was also increasing due to more hydrogen bonds being destroyed. The self-assembly behavior of **DNP1** in mixed $CDCl_3$/DMSO-d_6 solvent showed similar results (see ESI,† Fig. S6). However, **DNP1** started to open its ring when χ_{DMSO} was about 0.30, which is smaller than **DNP2**, further suggesting that the cyclic form of **DNP1** is less stable than **DNP2**.

Diffusion ordered NMR (DOSY) was further performed to study the self-assembly behaviors of **DNP1** and **DNP2**. The size of the self-assemblies was estimated by employing heptakis(2,3,6-tri-*O*-methyl)-β-cyclodextrin (peralkylated β-CD) as an internal standard. In the DOSY NMR spectrum, the larger the diffusion coefficient, the smaller the molecular weight of the assembly. As shown in Fig. 5a, the DOSY signal of **DNP1** below the CPC was regular and the diffusion coefficient (9.33×10^{-10} m^2 s^{-1}, 24 mM, MW = 805 Da, 2MW = 1610 Da) displayed a larger value than peralkylated β-CD (6.31×10^{-10} m^2 s^{-1}, MW = 1429 Da), indicating that the molecular weights of **DNP1** assemblies are smaller than 1429 Da and **DNP1** indeed existed as cyclic monomers in solution below the CPC. In stark contrast, the signals for **DNP1** in concentrated solution above CPC (350 mM) exhibited a wide distribution, suggesting a broad molecular weight distribution of assemblies (Fig. 5b and see Fig. 6 for details).

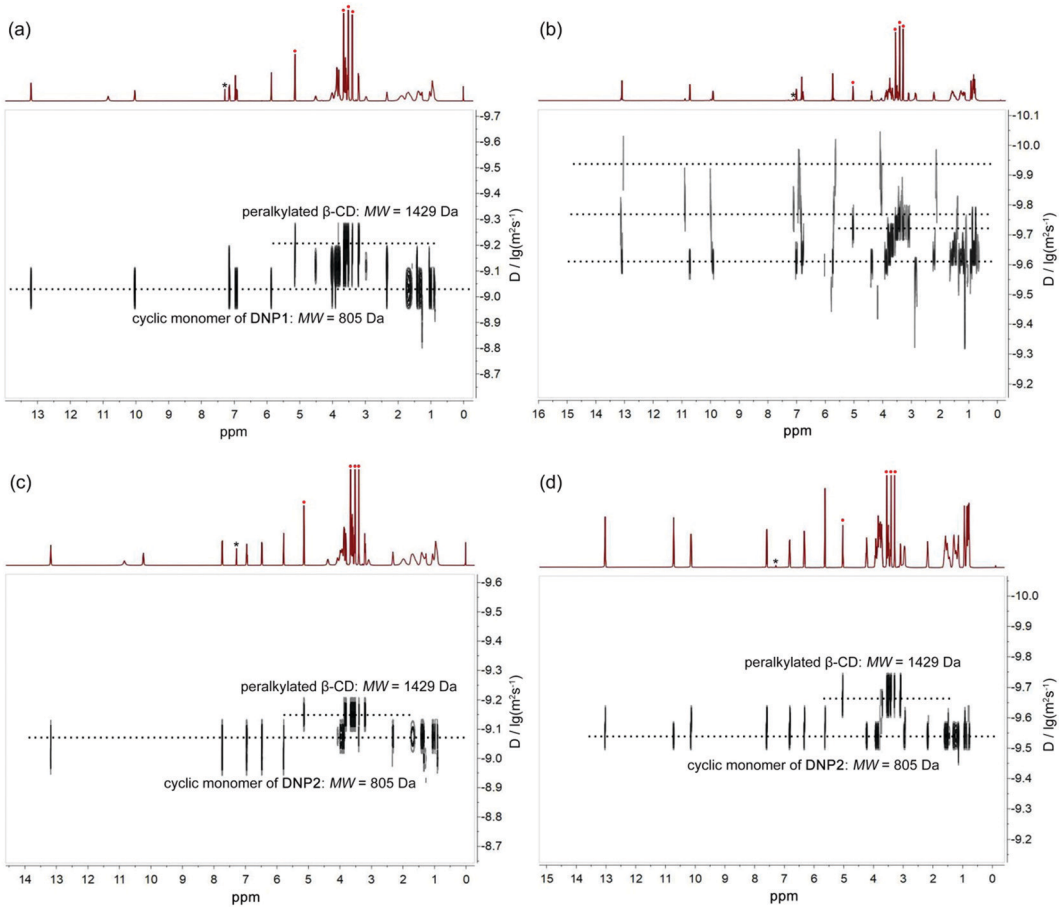

Fig. 5 DOSY spectra (600 MHz, $CDCl_3$, 298 K) of (a) **DNP1** in 24 mM, (b) **DNP1** in 350 mM, (c) **DNP2** in 24 mM and (d) **DNP2** in 350 mM. Peralkylated β-CD was added to each sample as internal standard. The asterisk symbols indicate solvent peaks and the red dots stand for proton signals from peralkylated β-CD.

The DOSY signals of **DNP2** both in dilute solution (24 mM, Fig. 5c) and concentrated solution (350 mM, Fig. 5d) displayed a well-defined narrow distribution and their diffusion coefficients were also larger than peralkylated β-CD. These phenomena indicate that **DNP2** always maintains a stable cyclic monomer structure, which is consistent with the results of variable concentration ^{1}H NMR and NOESY.

In order to better understand the self-assembly behavior of **DNP1** at relatively high concentration, a partially enlarged view of Fig. 5b was shown in Fig. 6. Proton signals from N—*H* involved in hydrogen bonding are mainly concerned. A wide distribution was clearly observed, indicating the formation of various assemblies with different size, including monomer (2.45×10^{-10} m^2 s^{-1}, MW = 805 Da), dimer (1.58×10^{-10} m^2 s^{-1}, MW = 1610 Da), and other larger aggregates (1.12×10^{-10} m^2 s^{-1}, MW > 1610 Da). Herein, the signals of the β-CD (1.86×10^{-10} m^2 s^{-1}, MW = 1429 Da) fell just in the middle of the signals of the monomer (MW = 805 Da) and the dimer (MW = 1610 Da), which further confirms our hypothesis.

The supramolecular polymerizability of **DNP1** and **DNP2** was further tested by viscosity measurements in $CHCl_3$. Double logarithmic plots of specific viscosity *versus* monomer concentration are shown in Fig. 7. For **DNP1**, a slope of 1.01 was found

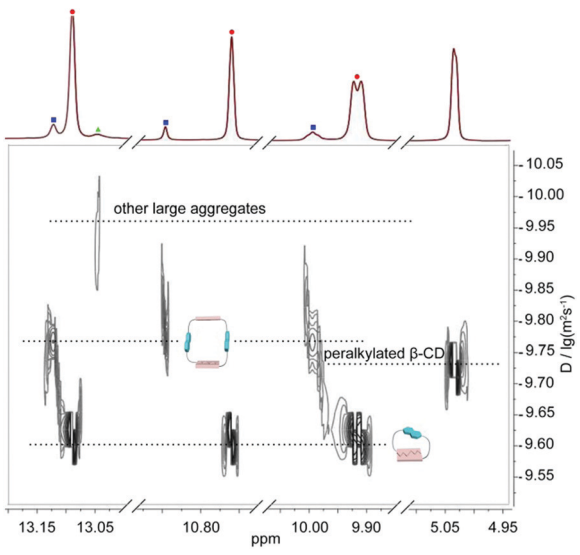

Fig. 6 Enlarged DOSY profile (600 MHz, $CDCl_3$, 298 K) of **DNP1** in 350 mM with the addition of peralkylated β-CD as internal standard. The red dots indicate cyclic monomers and the blue squares stand for cyclic dimers and the green triangles represent polymeric assemblies.

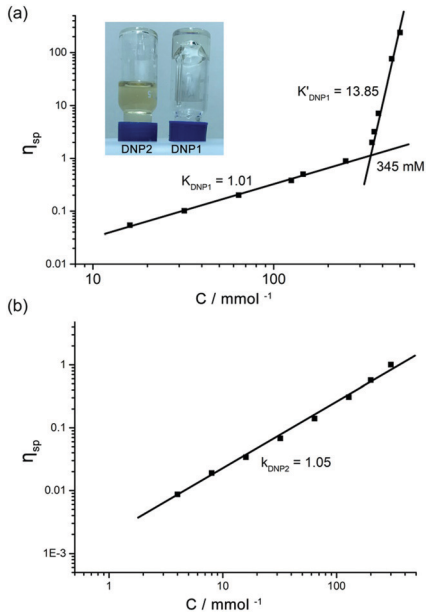

Fig. 7 Specific viscosity of chloroform solutions of (a) **DNP1** and (b) **DNP2** *versus* the monomer concentration (298 K). Values on the curves indicate the slope. Inset: Concentrated solution of **DNP1** (650 mM) and **DNP2** (650 mM) in $CHCl_3$.

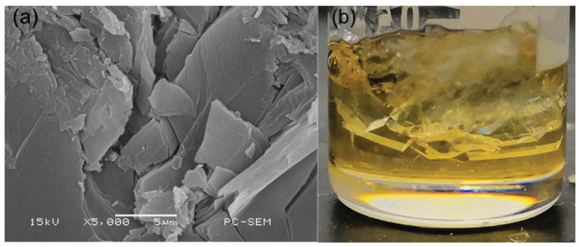

Fig. 8 (a) SEM image of the microscopic crystals of **DNP2** and (b) photograph of crystals precipitated from a concentrated solution (650 mM, in $CHCl_3$) of **DNP2**.

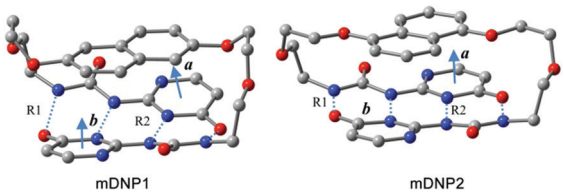

Fig. 9 The optimized structures representing models **mDNP1** and **mDNP2**. Color legend: red for O, blue for N, and grey for C. H atoms have been omitted for clarification. ***a*** and ***b*** represent the planar vectors of UPy moieties. All the optimized structures have C_2 symmetry.

in the initial stage upon concentration increasing, which is characteristic of cyclic monomers with constant size. As the concentration increased, a turning point occurred at 345 mM (CPC), which is close to the CPC determined by ^{1}H NMR measurements (347 mM). It is noteworthy that an extremely high slope of viscosity (k'_{DNP1} = 13.85) was obtained, indicating the formation of entangled supramolecular polymers with high molecular weight in concentrated solution. To the best of our knowledge, this slope value is the highest one for bifunctional UPy compounds.[13,52] The inset in Fig. 7a directly showed a highly viscous solution of **DNP1** (650 mM) in $CHCl_3$. Due to the relatively high CPC, the extra monomers will undergo rapid ring-opening polymerization to form large aggregates once the concentration reached the CPC. In contrast, **DNP2** showed a yellowish solution with good fluidity, even in very concentrated solutions (650 mM), implying that supramolecular polymerization did not occur. The viscosity profile of **DNP2** further explained this special phenomenon. As shown in Fig. 7b, the line displayed no turning point and the slope was 1.05 over the entire measurable range of concentration (0–300 mM), suggesting that a highly stable cyclic monomer always existed in solution, which was in line with concentration-dependent ^{1}H NMR. Attempts to test at higher concentrations (>300 mM) had failed because **DNP2** readily crystallized in the capillary of the viscometer. However, this phenomenon gave us another surprising conclusion that **DNP2** could easily crystallize out from its concentrated solution, indicating a totally different physicochemical property. Moreover, crystals with larger size were also found in a vial after partial evaporation of solvent from a concentrated solution of **DNP2** (Fig. 8b). A microscopic view of the crystals was further recorded by SEM (Fig. 8a).

The density functional theory studies of the representative models of **mDNP1** (for **DNP1**) and **mDNP2** (for **DNP2**) reveal that the total energy of **mDNP1** is about 12.4 kcal mol^{-1} higher than that of **mDNP2** (Fig. 9). This energy difference can be attributed to the stress of the strained ring or/and the energy difference between the 1,5-di-substituted naphthalene and the 2,6-di-substituted naphthalene. Further calculations of 1,5-dimethoxylnaphthalene and 2,6-dimethoxylnaphthalene indicate that 1,5-disubstituted naphthalene is only 0.6 kcal mol^{-1} more stable than 2,6-disubstituted naphthalene in energy. Thus, the additional energetic contribution to the destabilization of **mDNP1** (as compared to **mDNP2**) is due to the stress of the strained ring system. The optimized structures of **mDNP1** and **mDNP2** (Fig. 9 and Table 1) expose that although the H-bond lengths are similar for both compounds, the planes of H-bonding UPy moieties in **mDNP1** are highly twisted. The angle of the planar vectors of UPy moieties amounts to 25.7° in **mDNP1**, while this angle is 8° in **mDNP2**. The stress of the strained ring system of **mDNP1** reduces the H-bonding energy of the UPy moieties by about 11.8 kcal mol^{-1}.

Since the DNP moiety is a well-known electron rich group which can complex with electron deficient macrocycles to form

Table 1 The main geometric parameters of the fully optimized structures of model complexes **mDNP1** and **mDNP2**[a]

Model	mDNP1	mDNP2
R1	2.79	2.80
R2	2.99	3.01
θ	25.7	8.0

[a] R1 and R2 (in Å) are the H-bond distances (see Fig. 9), and θ (in degrees) is the angle between the planar vectors ***a*** and ***b*** of UPy moieties.

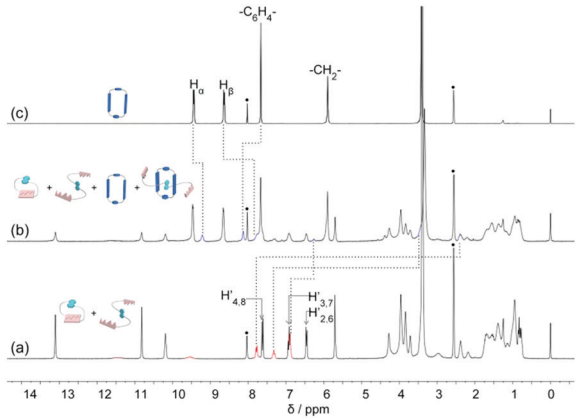

Fig. 10 Partial ^{1}H NMR spectra (300 MHz, $CDCl_3$/DMSO-d_6, v/v, χ_{DMSO} = 0.45) of: (a) **DNP2**, (b) **DNP2** (10 mM) and blue-box (10 mM), and (c) blue-box. The black dots stand for solvent peaks. Red peaks indicate open monomers of **DNP2**. Blue peaks represent the host–guest complex.

mechanically interlocked molecules, such as rotaxanes and catenanes, we envisioned what differences would happen in the host–guest complexation of **DNP1** and **DNP2** with a blue-box. We first investigated these molecules in mixed $CDCl_3$/CD_3CN solvent, hoping that the hydrogen bonds were not destroyed. However, at a low concentration (16 mM) both **DNP1** and **DNP2** showed no host–guest complexations with the blue-box, even after three days of reflux. This might be due to the high stability of these cyclic structures. Subsequently, we suspected that **DNP1** would bind with the blue-box at a high concentration (350 mM), where **DNP1** would open its ring owing to ring-opening supramolecular polymerization. However, the poor solubility of **DNP1** and the blue-box in mixed $CDCl_3$/CD_3CN impeded the investigation. Then, we studied the host–guest behaviors of **DNP1** and **DNP2** in mixed $CDCl_3$/DMSO-d_6 solvent. The results showed that only those open monomers could thread into the blue-box. For **DNP2**, even at χ_{DMSO} = 0.40, no bonded species were observed (see ESI,† Fig. S8) but at χ_{DMSO} = 0.45, obvious peaks representing pseudorotaxanes were observed (Fig. 10). Protons from DNP (H-2/6, H-3/7 and H-4/8) and the blue-box (H_α and H_β) exhibited large upfield shifts (blue peaks in Fig. 10b), indicating that the DNP moiety was encircled by the blue-box. In pure DMSO, the threading efficiency was up to 44% for **DNP2** (see ESI,† Fig. S8). In contrast, **DNP1** showed less affinity to the blue-box. Even in pure DMSO, only 14% blue-box was complexed with **DNP1** (see ESI,† Fig. S7). This should be due to the different association constants of 1,5-DNP and 2,6-DNP with the blue-box.

Conclusions

In conclusion, we have demonstrated a dramatic difference in supramolecular polymerizability for two structurally similar building blocks. The 2,6-substituted monomer **DNP1** possesses excellent supramolecular polymerizability, leading to the formation of highly viscous supramolecular polymers. The 1,5-substituted monomer **DNP2** lacks supramolecular polymerizability, resulting in the production of highly stable cyclic monomers with the capability of precipitation of crystals. Their different self-assembly behaviors have been thoroughly investigated by a series of techniques including concentration-dependent ^{1}H NMR, temperature-dependent ^{1}H NMR, mixed deuterated solvent ^{1}H NMR, NOESY, DOSY, SEM, viscosity measurements and theoretical calculations. Moreover, the host–guest complexation experiments showed that **DNP2** had a stronger binding ability with a blue-box than **DNP1** to form pseudorotaxanes when the hydrogen bonding was disrupted by addition of the hydrogen bond breaking solvent DMSO. The findings in this work will offer inspiration on supramolecular engineering and dynamic materials design. The construction of quadruple hydrogen bonded polyrotaxanes is ongoing in our laboratory.

Conflicts of interest

There are no conflicts to declare.

Acknowledgements

We gratefully acknowledge the financial support from the National Natural Science Foundation of China (21702020, 21572026) and the Advanced Catalysis and Green Manufacturing Collaborative Innovation Center (ACGM2016-06-05).

Notes and references

1 G. Vantomme and E. W. Meijer, *Science*, 2019, **363**, 1396–1397.
2 Z. Chen, Y. Liu, W. Wagner, V. Stepanenko, X. Ren, S. Ogi and F. Würthner, *Angew. Chem., Int. Ed.*, 2017, **56**, 5729–5733.
3 J. Kang, D. Miyajima, T. Mori, Y. Inoue, Y. Itoh and T. Aida, *Science*, 2015, **347**, 646–651.
4 F. Würthner, T. E. Kaiser and C. R. Saha-Möller, *Angew. Chem., Int. Ed.*, 2011, **50**, 3376–3410.
5 Q.-F. Sun, J. Iwasa, D. Ogawa, Y. Ishido, S. Sato, T. Ozeki, Y. Sei, K. Yamaguchi and M. Fujita, *Science*, 2010, **328**, 1144–1147.
6 B. Adelizzi, N. J. Van Zee, L. N. J. de Windt, A. R. A. Palmans and E. W. Meijer, *J. Am. Chem. Soc.*, 2019, **141**, 6110–6121.
7 X. Yan, F. Wang, B. Zheng and F. Huang, *Chem. Soc. Rev.*, 2012, **41**, 6042–6065.
8 T. Aida, E. W. Meijer and S. I. Stupp, *Science*, 2012, **335**, 813–817.
9 L. Brunsveld, B. J. Folmer, E. W. Meijer and R. P. Sijbesma, *Chem. Rev.*, 2001, **101**, 4071–4098.
10 L. Herkert, J. Droste, K. K. Kartha, P. A. Korevaar, T. F. A. de Greef, M. R. Hansen and G. Fernandez, *Angew. Chem., Int. Ed.*, 2019, **58**, 11344–11349.
11 P. A. Korevaar, S. J. George, A. J. Markvoort, M. M. J. Smulders, P. A. J. Hilbers, A. P. H. J. Schenning, T. F. A. De Greef and E. W. Meijer, *Nature*, 2012, **481**, 492–496.
12 T. Xiao, L. Zhou, X.-Q. Sun, F. Huang, C. Lin and L. Wang, *Chin. Chem. Lett.*, 2019, DOI: 10.1016/j.cclet.2019.05.011.
13 T. Xiao, W. Zhong, L. Qi, J. Gu, X. Feng, Y. Yin, Z.-Y. Li, X.-Q. Sun, M. Cheng and L. Wang, *Polym. Chem.*, 2019, **10**, 3342–3350.

14 P. Wei, X. Yan and F. Huang, *Chem. Soc. Rev.*, 2015, **44**, 815–832.
15 X. Ma, Y. Zhang, Y. Zhang, Y. Liu, Y. Che and J. Zhao, *Angew. Chem., Int. Ed.*, 2016, **55**, 9539–9543.
16 S. Ogi, V. Stepanenko, K. Sugiyasu, M. Takeuchi and F. Würthner, *J. Am. Chem. Soc.*, 2015, **137**, 3300–3307.
17 D.-S. Guo and Y. Liu, *Acc. Chem. Res.*, 2014, **47**, 1925–1934.
18 S. Dong, B. Zheng, F. Wang and F. Huang, *Acc. Chem. Res.*, 2014, **47**, 1982–1994.
19 Q. Zhang, T. Li, A. Duan, S. Dong, W. Zhao and P. J. Stang, *J. Am. Chem. Soc.*, 2019, **141**, 8058–8063.
20 S. G. Chen, Y. Yu, X. Zhao, Y. Ma, X. K. Jiang and Z. T. Li, *J. Am. Chem. Soc.*, 2011, **133**, 11124–11127.
21 S. Datta, M. L. Saha and P. J. Stang, *Acc. Chem. Res.*, 2018, **51**, 2047–2063.
22 K. C. Bentz and S. M. Cohen, *Angew. Chem., Int. Ed.*, 2018, **57**, 14992–15001.
23 L. Xu, X. Shen, Z. Zhou, T. He, J. Zhang, H. Qiu, M. L. Saha, S. Yin and P. J. Stang, *J. Am. Chem. Soc.*, 2018, **140**, 16920–16924.
24 Q. Wang, M. Cheng, L. Tian, Q. Fan and J. Jiang, *Polym. Chem.*, 2017, **8**, 6058–6063.
25 H. Wang, X. Ji, Z. Li, C. N. Zhu, X. Yang, T. Li, Z. L. Wu and F. Huang, *Mater. Chem. Front.*, 2017, **1**, 167–171.
26 L. J. Chen and H. B. Yang, *Acc. Chem. Res.*, 2018, **51**, 2699–2710.
27 A. T. t. Cate and R. P. Sijbesma, *Macromol. Rapid Commun.*, 2002, **23**, 1094–1112.
28 R. P. Sijbesma, F. H. Beijer, L. Brunsveld, B. J. B. Folmer, J. H. K. K. Hirschberg, R. F. M. Lange, J. K. L. Lowe and E. W. Meijer, *Science*, 1997, **278**, 1601–1604.
29 F. H. Beijer, R. P. Sijbesma, H. Kooijman, A. L. Spek and E. W. Meijer, *J. Am. Chem. Soc.*, 1998, **120**, 6761–6769.
30 X. Zhu, J. X. Wang, L. Y. Niu and Q. Z. Yang, *Chem. Mater.*, 2019, **31**, 3573–3581.
31 S. J. Rao, K. Nakazono, X. Liang, K. Nakajima and T. Takata, *Chem. Commun.*, 2019, **55**, 5231–5234.
32 X. Yan, Z. Liu, Q. Zhang, J. Lopez, H. Wang, H. C. Wu, S. Niu, H. Yan, S. Wang, T. Lei, J. Li, D. Qi, P. Huang, J. Huang, Y. Zhang, Y. Wang, G. Li, J. B. Tok, X. Chen and Z. Bao, *J. Am. Chem. Soc.*, 2018, **140**, 5280–5289.
33 W.-J. Liang, J.-J. Yu, Q. Zhang, C.-S. Ma, Z.-T. Shi and D.-H. Qu, *Polym. Chem.*, 2018, **9**, 4808–4812.
34 A. Lavrenova, D. W. R. Balkenende, Y. Sagara, S. Schrettl, Y. C. Simon and C. Weder, *J. Am. Chem. Soc.*, 2017, **139**, 4302–4305.
35 A. Goujon, G. Mariani, T. Lang, E. Moulin, M. Rawiso, E. Buhler and N. Giuseppone, *J. Am. Chem. Soc.*, 2017, **139**, 4923–4928.
36 T. Xiao, L. Xu, J. Wang, Z.-Y. Li, X.-Q. Sun and L. Wang, *Org. Chem. Front.*, 2019, **6**, 936–941.
37 Q. Chen, X. Su, E. Orentas and Q. Shi, *Org. Chem. Front.*, 2019, **6**, 611–617.
38 H.-Q. Peng, X. Zheng, T. Han, R. T. K. Kwok, J. W. Y. Lam, X. Huang and B. Z. Tang, *J. Am. Chem. Soc.*, 2017, **139**, 10150–10156.
39 Z. Chen, A. Lohr, C. R. Saha-Möller and F. Würthner, *Chem. Soc. Rev.*, 2009, **38**, 564–584.
40 C. A. Hunter and J. K. M. Sanders, *J. Am. Chem. Soc.*, 1990, **112**, 5525–5534.
41 T. Xiao, X. Feng, S. Ye, Y. Guan, S.-L. Li, Q. Wang, Y. Ji, D. Zhu, X. Hu, C. Lin, Y. Pan and L. Wang, *Macromolecules*, 2012, **45**, 9585–9594.
42 D. Guo, R. P. Sijbesma and H. Zuilhof, *Org. Lett.*, 2004, **6**, 3667–3670.
43 K. Liu, C. Wang, Z. Li and X. Zhang, *Angew. Chem., Int. Ed.*, 2011, **50**, 4952–4956.
44 T. Xiao, W. Zhong, L. Zhou, L. Xu, X.-Q. Sun, R. B. P. Elmes, X.-Y. Hu and L. Wang, *Chin. Chem. Lett.*, 2019, **30**, 31–36.
45 T. Xiao, L. Xu, L. Zhou, X.-Q. Sun, C. Lin and L. Wang, *J. Mater. Chem. B*, 2019, **7**, 1526–1540.
46 T. Xiao and L. Wang, *Tetrahedron Lett.*, 2018, **59**, 1172–1182.
47 T. F. A. D. Greef, M. M. J. Smulders, M. Wolffs, A. P. H. J. Schenning, R. P. Sijbesma and E. W. Meijer, *Chem. Rev.*, 2009, **109**, 5687–5754.
48 J. F. Stoddart, *Angew. Chem., Int. Ed.*, 2017, **56**, 11094–11125.
49 S. Dasgupta and J. Wu, *Chem. Sci.*, 2012, **3**, 425–432.
50 R. S. Forgan, J.-P. Sauvage and J. F. Stoddart, *Chem. Rev.*, 2011, **111**, 5434–5464.
51 S.-L. Li, T. Xiao, W. Xia, X. Ding, Y. Yu, J. Jiang and L. Wang, *Chem. – Eur. J.*, 2011, **17**, 10716–10723.
52 O. A. Scherman, G. B. W. L. Ligthart, R. P. Sijbesma and E. W. Meijer, *Angew. Chem., Int. Ed.*, 2006, **45**, 2072–2076.